Deformation of Semi-Solid Sn-15 Pct Pb Alloy

V. LAXMANAN AND M. C. FLEMINGS

The rheological behavior of semisolid Sn-15 pct Pb alloy was studied using a parallel-plate viscometer. Small nondendritic and dendritic semisolid samples of the alloy were deformed under a constant load at initial pressures up to 232 kPa (33.6 psi) and at fractions solid from 0.15 to 0.60. Strain-time data for the nondendritic material obey the non-Newtonian, two-parameter, Ostwald-de-Waele, power-law model, *i.e.* $\mu = m\dot{\gamma}^{n-1}$, where μ is viscosity, $\dot{\gamma}$ shear rate and m and n are constants. For fractions solid above about 0.30, the following empirical equation relates viscosity, shear rate and fraction solid

$$\mu = a \exp(bf_s)\, \dot{\gamma}^{(cf_s+d)} \quad 0.3 < f_s < 0.60$$

where f_s is fraction solid and a, b, c, d are constants. The nondendritic alloy deformed homogeneously without cracking to very large strains (up to 80 pct). Dendritic alloys required much higher loads and cracked easily. For the nondendritic alloys the forging pressures to obtain 50 pct compression were of the order of 7 to 70 kPa (1 to 10 psi) for fractions solid under 0.55 and 172.5 to 207 kPa (25 to 30 psi) for fraction solid of about 0.60. For the dendritic alloys, the forging pressure required to achieve 10 pct compression is about 85 kPa at a fraction solid of 0.35 and increases rapidly with increasing fraction solid.

OVER the last few years a new class of metal forming processes has been developed[1-9] which rely on the fact that with vigorous agitation during the early stages of solidification, the primary solid which forms has a nondendritic structure. As a result, the semisolid behaves as a "thixotropic" slurry. That is, the viscosity of the alloy shows a time dependency and decreases with increasing shear rates. The semisolid alloys retain their fluid-like behavior well into the liquid-solid range and can be successfully formed or shaped in this region.

The process which utilizes the slurry formed as above has been termed "Rheocasting". Alternatively, the slurry may be fully solidified and later partially remelted without agitation. On shearing, it again assumes its fluid character, and so can be cast under pressure ("Thixocast"), forged ("Thixoforged"), rolled or extruded. Rheocasting and Thixocasting have been successfully employed for machine casting copper-base alloys[5] and high temperature ferrous alloys such as AISI 440C stainless steel[6] and AISI 4340 low alloy steel.[7]

The central aim of this work is to study the rheological behavior of partially remelted nondendritic or "Thixocast" alloys. Previous fundamental work on the rheological behavior of nondendritic alloys[8,9] has been confined to the original slurry (or Rheocast material). Figure 1 from Joly and Mehrabian is an example from that work.[9]

In this work, a compression apparatus similar to a parallel-plate viscometer was used to study the deformation behavior of Thixocast Sn-15 pct Pb alloy over a wide range of temperatures within the liquid-solid range. In this instrument, the semisolid alloy is squeezed under a constant load between two parallel disks, as shown schematically in Fig. 2(*a*), and the viscosity is calculated from the strain-time curve obtained during compression such as the one shown schematically in Fig. 2(*b*). Devices employing this geometry have been used previously for quality control tests on materials such as asphalts and rubbers and in studying the deformation behavior of many plastics and polymers.[10-16] Since the test resembles closely an open die-forging operation, it also provides useful engineering information on the deformability of partially solid alloys.

EXPERIMENTAL PROCEDURE

Figure 3 is a schematic diagram of the compression apparatus used in this investigation. The compression plates are located in the center of a hollow stainless steel furnace (30 cm long, 3.75 cm diam, 1.6 mm wall thickness), open at both ends. Power is supplied by four 200 W bandheaters spaced evenly along the furnace tube and the entire assembly is heavily insulated. The two compression plates are made of stainless steel disks, 12.5 mm thick, accurately machined to provide a diametral clearance of approximately 13 thousandths of a centimeter (0.005 in.) between the plates and the furnace tube.

A linear voltage displacement transducer is used to obtain the displacement as a function of time during compression. The output voltage of the transducer is continuously recorded on a strip chart recorder. Four chromel-alumel thermocouples are used to assure temperature uniformity in the test specimen. Two are embedded in the bottom plate, about 1.5 mm from the compression face, one in the top plate, 1.5 mm from the compression face, and one in a small hole drilled through the center of the top plate. This last thermocouple is almost in direct contact with the metal. One thermocouple, placed along the shaft attached to the top plate, serves as the control thermocouple, in conjunction with a solid-state temperature controller, to regulate the heat input to the furnace. Temperature uniformity in the test specimen is further aided by small

V. LAXMANAN is Postdoctoral Associate and M. C. FLEMINGS is Ford Professor of Engineering, Department of Materials Science and Engineering, Massachusetts Institute of Technology, Cambridge, MA 02139.

Manuscript submitted January 25, 1980.

ISSN 0360-2133/80/1211-1927$00.75/0

heating coils wound around the stainless steel shafts attached to the compression plates. Adjustment of the heat input to these coils made it possible to maintain the temperature in the region between the two compression plates to within ±1 °C throughout a test. In experiments conducted at the lower fractions solid (<0.40), where the fraction solid-temperature curve is steeper, special care was taken to hold the temperature to within ±0.5 °C.

Test specimens were all of Sn-15 pct Pb alloy, and were cylindrical, 1.25 cm diam and 0.625 cm high (0.500 in. diam, 0.250 in. high). The majority were nondendritic, ("Rheocast"), machined from ingots made in a low-temperature slurry producer.[17,18] A few experiments were also carried out with equiaxed dendritic alloys, columnar dendritic alloys with dendrites grown along the axis of the specimen cylinder and, finally, with the columnar dendrites grown perpendicular to the axis of the cylinder. Tests were conducted over a range of fractions solid of 0.15 to 0.60; the compressive loads applied varied between 10 grams and 3000 grams. At each fraction solid studied, compression was carried out with at least two different loads and in most cases,

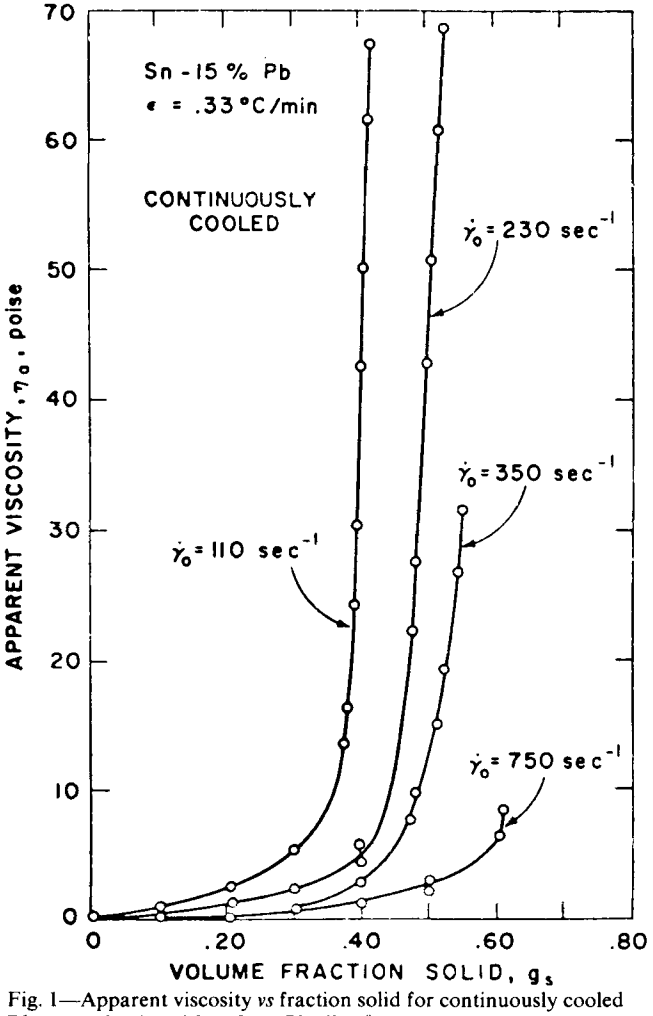

Fig. 1—Apparent viscosity *vs* fraction solid for continuously cooled Rheocast slurries of Sn-15 pct Pb alloy.[9]

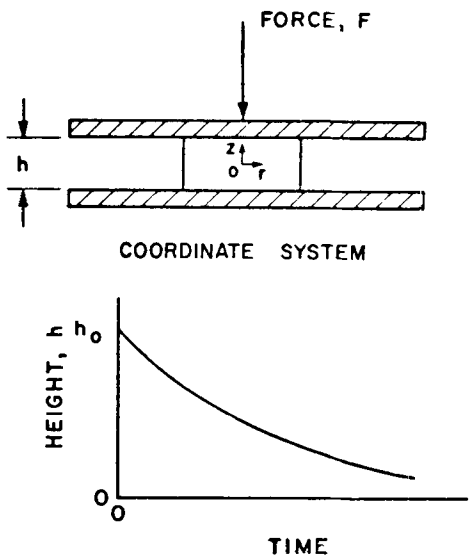

Fig. 2—Schematic diagram of parallel-plate viscometer. (*a*) compression test, (*b*) height *vs* time during compression.

Test specimens were all of Sn-15 pct Pb alloy, and were cylindrical, 1.25 cm diam and 0.625 cm high (0.500 in. diam, 0.250 in. high). The majority were nondendritic, ("Rheocast"), machined from ingots made in a low-temperature slurry producer.[17,18] A few experiments were also carried out with equiaxed dendritic alloys, columnar dendritic alloys with dendrites grown along the axis of the specimen cylinder and, finally, with the columnar dendrites grown perpendicular to the axis of the cylinder. Tests were conducted over a range of fractions solid of 0.15 to 0.60; the compressive loads applied varied between 10 grams and 3000 grams. At each fraction solid studied, compression was carried out with at least two different loads and in most cases,

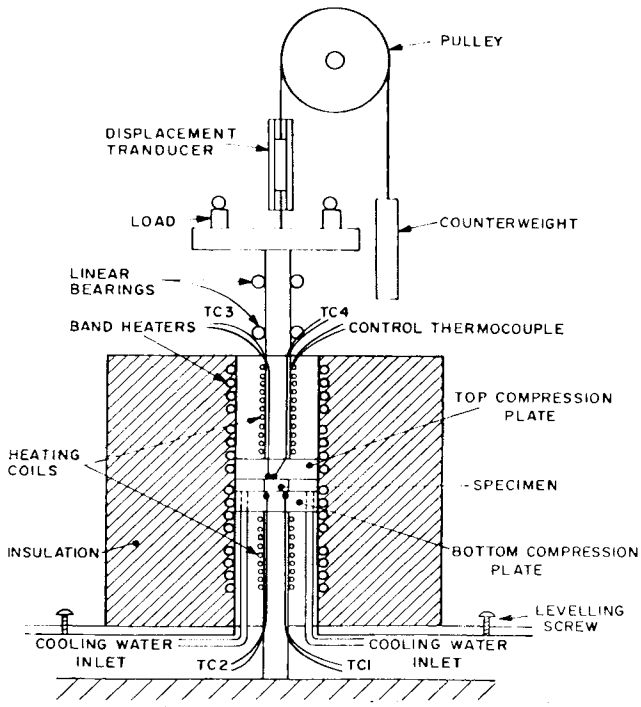

Fig. 3—Schematic diagram of experimental apparatus.

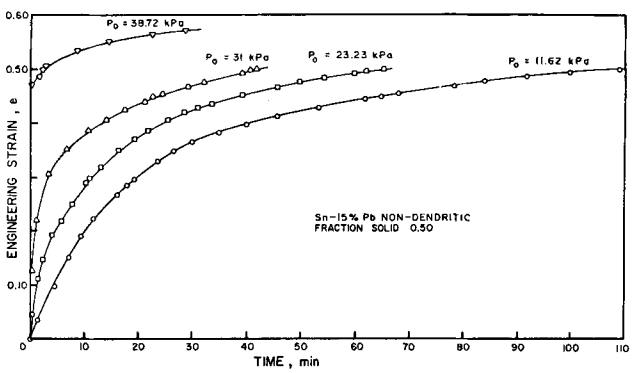

Fig. 4—Typical strain-time curves for partially remelted Sn-15 pct Pb nondendritic alloy. Fraction solid, f_s = 0.50. Tests conducted at four different initial pressures.

especially with nondendritic alloys, with four different loads. Typically, compression was continued to a strain of 0.50. The specimen was then quenched in place by turning on the cooling water which flowed around the specimen and cooled it far below the eutectic temperature within a few seconds.

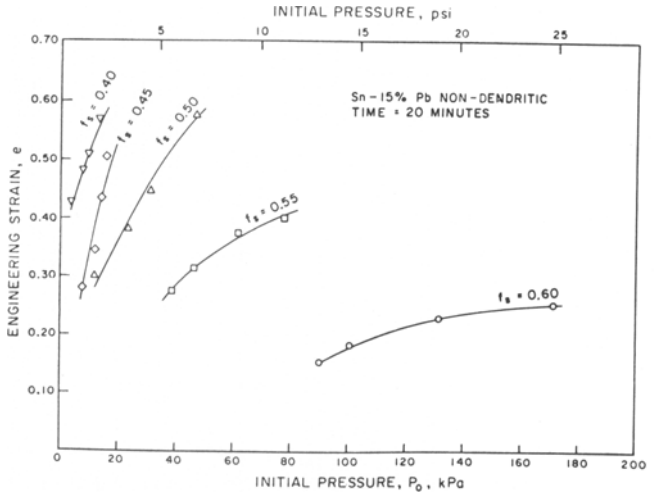

Fig. 5—Engineering strain at 20 min *vs* initial pressure. Nondendritic samples.

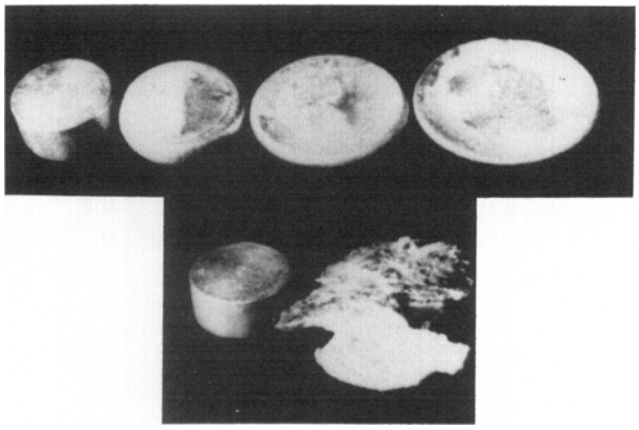

Fig. 6—Photographs of typical test samples. Top row: Nondendritic samples with increasing amount of strain from left to right, P_0 = 11.62 kPa, f_s = 0.50. Bottom row: Equiaxed dendritic sample, P_0 = 183 kPa, f_s = 0.35 before and after squeezing.

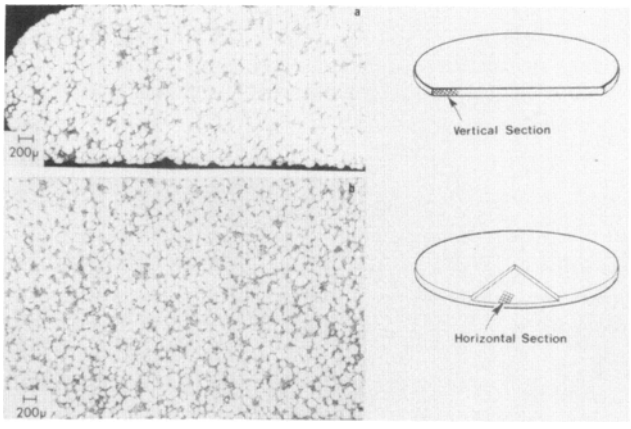

Fig. 7—Typical microstructures of deformed nondendritic sample. P_0 = 38.72 kPa, f_s = 0.50, and final strain e = 0.58. (*a*) Vertical section, (*b*) horizontal section.

EXPERIMENTAL RESULTS

A. Engineering Studies

Figure 4 is a typical displacement-time curve obtained during compression with a nondendritic alloy. In this figure, displacement has been converted into engineering strain, e, defined as,

$$e = 1 - \frac{h}{h_0} \qquad [1]$$

where h_0 = initial height of specimen, h = instantaneous height during compression.

Fraction solid, f_s, was calculated using the Scheil equation,

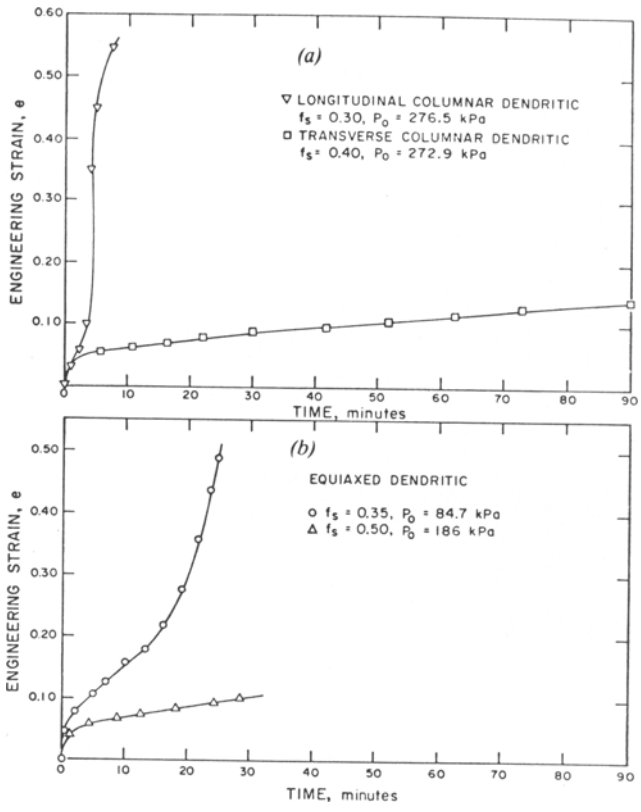

Fig. 8—Typical strain-time curves for dendritic samples (*a*) columnar dendritic, (*b*) equiaxed dendritic.

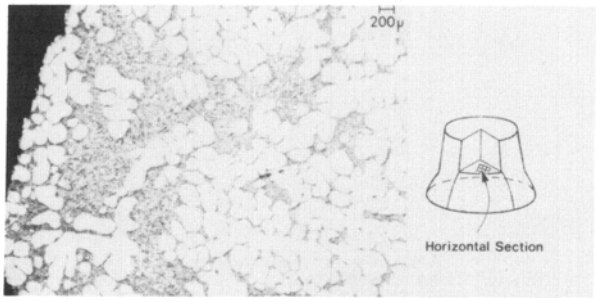

Fig. 9—Typical microstructure of deformed equiaxed dendritic sample. P_0 = 186 kPa, f_s = 0.50, and final strain = 0.15.

$$f_s = 1 - \left(\frac{T_M - T_L}{T_M - T}\right)^{1/1-k} \quad [2]$$

where k is the equilibrium partition ratio, T_M is the melting point of the pure solvent, T_L is the liquidus temperature of the alloy and T is the test temperature.

Since the specimen is squeezed under a constant load, the forging pressure decreases continuously during compression. The instantaneous forging pressure, P, is given by

$$P = \frac{Fh_0}{v}(1 - e) \quad [3]$$

where v = volume of specimen, constant, F = applied load, and the initial forging pressure, P_0, is given by

$$P_0 = \frac{Fh_0}{v} \quad [4]$$

Strain as shown in Fig. 4 depends on time and the initial pressure, P_0. It also, of course, depends on fraction solid and Fig. 5 summarizes some strain data for different fraction solid (at constant time). Table I summarizes results from all experiments, including temperature, fraction solid, initial pressure and total strain at the end of each run.

The nondendritic specimens deformed without cracking as shown by the photographs in the top row of Fig. 6. Deformation was nearly homogeneous, with only very slightly more of the primary solid particles at the center of a sample than at the edges as seen in the photomicrographs of Fig. 7.

The dendritic samples deformed very differently from the nondendritic samples as seen from the strain-time data in Figs. 8(*a*) and (*b*). At the higher fractions solid,

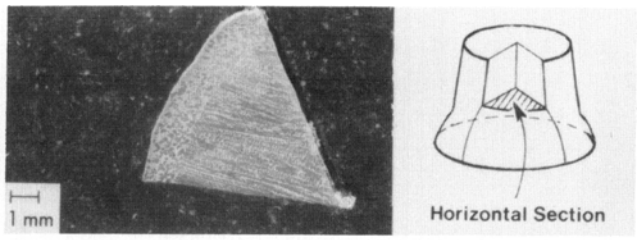

Fig. 10—Typical microstructures of columnar dendritic alloy deformed with stress axis perpendicular to dendritic growth direction. P_0 = 273 kPa, f_s = 0.40, final strain = 0.10. (Note exuded liquid layer.)

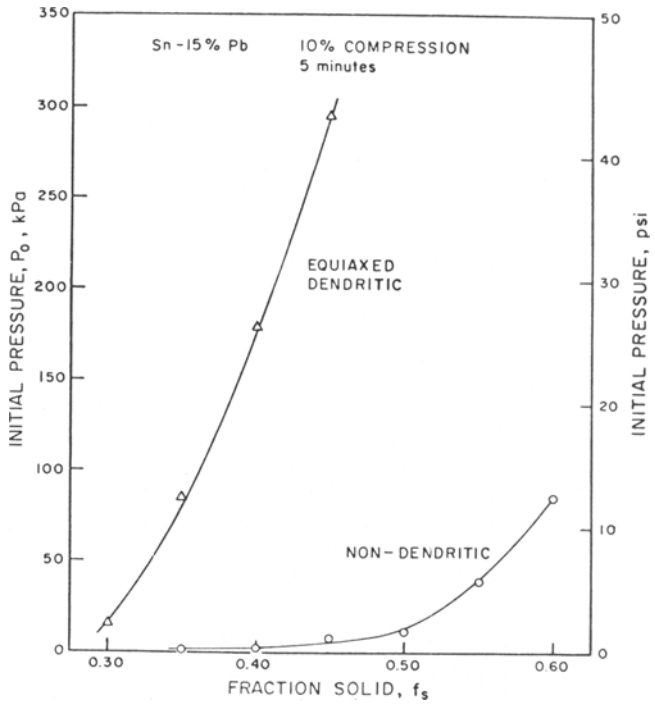

Fig. 11—Initial forging pressure, P_0, for a compressive strain of 0.10 in 5 min *vs* fraction solid for dendritic and nondendritic structures.

only small strains (<0.10) are obtained even at very long times for a given initial pressure. See, for example, the lower curves in both Figs. 8(*a*) and (*b*). For lower fractions solid (<0.35), however, the strain increases very slowly at first and then abruptly accelerates; this is shown by the upper curves of Figs. 8(*a*) and (*b*). This rapid increase in strain was found to be associated with visible cracks, such as seen in the photographs in the bottom row of Fig. 6, and/or exudation of liquid into cracks formed between dendrites or liquid flow out of the dendrites to the periphery of the sample as seen in the photomicrographs in Figs. 9 and 10.

Moreover, the forging pressures required to achieve a given amount of deformation in the dendritic samples are much higher than those for the corresponding nondendritic samples. This is shown in Fig. 11, which compares the initial forging pressure, P_0, to achieve a strain of 0.10 in 5 min at various fractions solid for the different types of structures. The pressures required with the nondendritic structure are approximately two orders of magnitude lower than for the dendritic structure.

B. Rheological Analysis—Newtonian Model

The simplest way to analyze the results obtained in this study is to assume that the semisolid alloy being squeezed behaves like a Newtonian fluid. Such an assumption would be a reasonable first approximation for a thixotropic material, provided the shear rates are low and do not vary greatly within the sample during the test. As will be seen later, the results obtained using this simplified model are closely similar to those obtained using the more appropriate "power law" model.

Consider the squeezing flow problem between two

Table I. Experimental Data

Experiment Number	Temperature, °C	Fraction Solid, f_s	Initial Pressure, kPa	Total Strain, e
Experiments on Nondendritic Structures				
1	186 ± 1	0.60	170.4	0.541
2	186 ± 1		132	0.456
3	186 ± 1		101	0.284
4	186 ± 1		85.2	0.271
5	191 ± 1	0.55	77.5	0.516
6	191 ± 1		62	0.502
7	191 ± 1		46.5	0.504
8	191 ± 1		38.75	0.503
9	194 ± 1	0.50	38.75	0.572
10	194 ± 1		31	0.492
11	194 ± 1		23.2	0.500
12	194 ± 1		11.6	0.506
13	197 ± 1	0.45	15.5	0.497
14	197 ± 1		13.6	0.484
15	197 ± 1		11.6	0.491
16	197 ± 1		7.75	0.504
17	198 ± 0.5	0.40	13.6	0.602
18	198 ± 0.5		9.3	0.551
19	198 ± 0.5		5.4	0.503
20	198 ± 0.5		3.9	0.505
21	200 ± 0.5	0.35	11.6	0.502
22	200 ± 0.5		7.75	0.502
23	200 ± 0.5		3.9	0.452
24	200 ± 0.5		3.1	0.405
25	202 ± 0.5	0.30	2.32	0.451
26	203.5 ± 0.5	0.25	3.9	0.507
27	203.5 ± 0.5		1.55	0.615
28	205 ± 0.5	0.20	1.55	0.666
29	205 ± 0.5		0.8	0.500
30	207 ± 0.5	0.15	0.8	0.556
Experiments on Equiaxed Dendritic Structures				
31	194 ± 1	0.50	186	0.152
32	197 ± 1	0.45	283.4	0.154
33	197 ± 1		180	0.151
34	198.5 ± 0.5	0.40	179.6	0.151
35	198.5 ± 0.5		98.8	0.138
36	198.5 ± 0.5		46.9	0.063
37	200 ± 0.5	0.35	183.2	0.603
38	200 ± 0.5		84.7	0.484
39	200 ± 0.5		80.3	0.318
40	200 ± 0.5		63.6	0.265
41	200 ± 0.5		38,1	0.313
42	202 ± 0.5	0.30	63.4	0.420
43	202 ± 0.5		42.7	0.379
Experiments on Longitudinal Columnar Dendritic Structures (growth direction parallel to stress axis)				
44	202 ± 0.5	0.30	281.2	0.163
45	202 ± 0.5		276.5	0.649
46	202 ± 0.5		185.8	0.617
47	205 ± 0.5	0.20	47	0.583
Experiments on Transverse Columnar Dendritic Structures (growth direction perpendicular to stress axis)				
48	198.5 ± 0.5	0.40	273	0.100
49	198.5 ± 0.5		139.3	0.051
50	202 ± 0.5	0.30	281.6	0.106

Fraction solid was calculated using Scheil equation with a constant partition ratio of $k = 0.10$.

plates where the material under test has an initial radius R_0, height h_0, at $t \leq 0$. A constant force, F, is now applied to the top plate and maintained for times $t > 0$. As a result, the plate separation, h, changes with time t, Fig. 2.

The original derivation for the plate separation equation for a Newtonian fluid is due to Stefan.[19] This solution was applied to the parallel-plate viscometer by Dienes and Klemm[10] and by Gearhart and Kennedy.[16] The differential form of their solution for the case when the fluid does not completely fill the space between the plates is:

$$F = -\frac{3\mu v^2}{2\pi h^5}\left(\frac{dh}{dt}\right) \qquad [5]$$

where μ is the viscosity of the fluid, v is the volume of

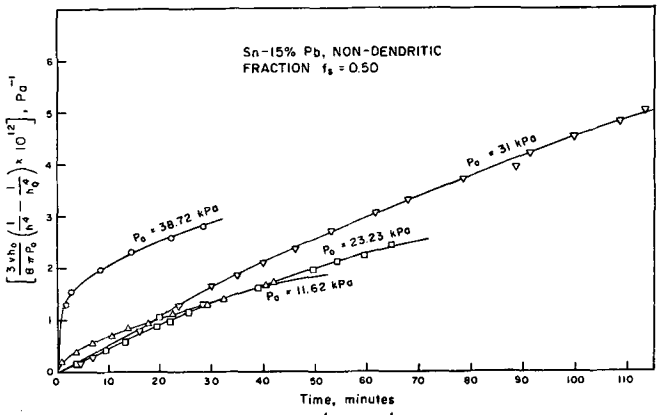

Fig. 12—Typical plot of $3\nu h_0(1/h^4 - 1/h_0^4)/8\pi P_0$ *vs* time for partially remelted nondendritic samples. Fraction solid, $f_s = 0.50$. Tests conducted at four different initial pressures.

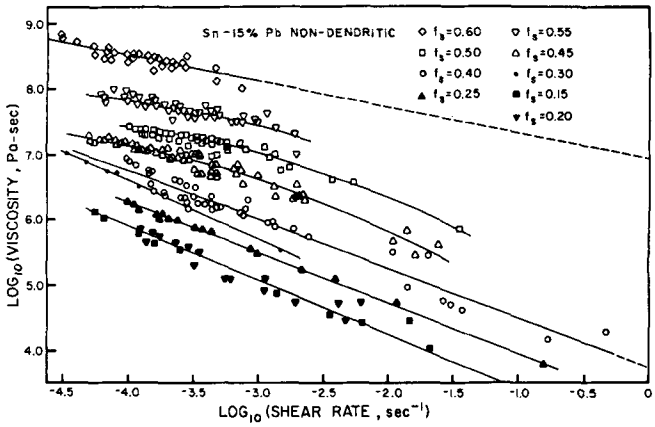

Fig. 13—Plot of calculated instantaneous Newtonian viscosity *vs* average shear rate for partially remelted nondendritic samples. Data obtained from tests conducted at different initial pressures for each fraction solid.

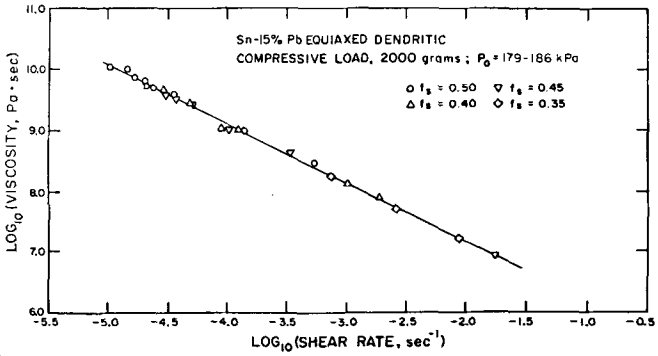

Fig. 14—Plot of calculated instantaneous Newtonian viscosity *vs* average shear rate for equiaxed dendritic samples deformed with a compressive load of 2000 grams (initial pressures between 179 to 186 kPa). Data obtained from tests conducted at different fractions solid and before any rapid increase in strain.

the material, h is the instantaneous height of the sample and t is time. In the usual case of the parallel-plate viscometer, the sample size is chosen equal to the platen size, so the area of compression remains constant during the test. In this work, the sample was always smaller than the platen area, and for this case, the solution of Eq. [5] was obtained by first integrating from $h = h_0$ at $t = 0$ to yield:

$$\frac{1}{h^4} - \frac{1}{h_0^4} = \frac{8\pi F t}{3\mu v^2} \quad [6]$$

Rewriting Eq. [6] and substituting [4] yields:

$$\frac{3vh_0}{8\pi P_0}\left(\frac{1}{h^4} - \frac{1}{h_0^4}\right) = \frac{t}{\mu} \quad [7]$$

Equation [6] indicates that the viscosity μ may be calculated by plotting $(1/h^4 - 1/h_0^4)$ *vs* time, t. This method was used by Dienes and Klemm to determine the viscosity of polyethylene and by Gearhart and Kennedy for molten polystyrene and cellulose acetate butyrate (*i.e.* at low shear rates where these materials exhibit simple Newtonian behavior).

Figure 12 is a typical plot of strain-time data, from this work, based on Eq. [7]. Viscosity is the reciprocal slope of this plot. It is seen to vary only slightly within a given test (after initial startup) and to vary more markedly with P_0. In using this Newtonian approximation to describe the data herein, the viscosity, instead, was calculated from the differential expression in Eq. [5] at several different times during the test.

For a Newtonian fluid, the shear rate, $\dot{\gamma}$, at any instant during compression is given by,

$$\dot{\gamma} = -\frac{6rz}{h^3}\frac{dh}{dt} \quad [8]$$

where r is the radial distance from the center of the specimen and z is the vertical distance from the centerline. The average shear rate, $\dot{\gamma}_{av}$, obtained by integrating throughout the volume is:

$$\dot{\gamma}_{av} = \frac{2\pi}{v}\int_0^R \int_0^{h/2} \dot{\gamma} r\, dr\, dz \quad [9]$$

Combining [8] and [9] and integrating yields:

$$\dot{\gamma}_{av} = -\frac{R}{2h^2}\frac{dh}{dt} \quad [10]$$

where R is the radius of the specimen at time, t.

Combining [10] and [5] and using $v = \pi R^2 h$ gives,

$$\dot{\gamma}_{av} = -\sqrt{\frac{v}{\pi}}\left(\frac{dh/dt}{2h^{2.5}}\right) \quad [11]$$

The maximum shear rate, $\dot{\gamma}_{max}$, obtained by substituting $r = R, z = h/2$ in Eq. [8] is

$$\dot{\gamma}_{max} = -\frac{3R}{h^2}\frac{dh}{dt} = 6\dot{\gamma}_{av} \quad [12]$$

In analyzing the experimental results, using the simpler Newtonian model, the viscosity was calculated directly from Eq. [5] and the average shear rate from Eq. [11].

Figure 13 is a plot of these calculated viscosities and shear rates for all the nondendritic runs listed in Table I. It may be seen that the viscosity decreases with increasing shear rate at constant fraction solid, indicating that the material is not Newtonian. Moreover, the data points lie along straight lines over a range of shear rates greater than 3 orders of magnitude, while the viscosity itself varies by as much as 2 orders of magnitude.

Perhaps surprisingly, data for the equiaxed dendritic specimens (before cracking) also plotted linearly *vs* the average shear rate. This is shown in Fig. 14. Calculations were made along points on the strain curves before the rapid increase in strain rate that is associated with cracking or segregate formation.

C. Rheological Analysis—Power Law Model

The non-Newtonian, two-parameter, Ostwald-de-Waele or "power-law" model is widely used to describe the rheological behavior of pseudoplastic materials and has been used for a number of liquid-solid slurries, including clay-water-oil slurries, polymer blends and filled polymers.[22-26] This model assumes a relationship of the form,

$$\mu = m\dot{\gamma}^{(n-1)} \quad [13]$$

where m and n are experimentally determined constants.

The original solution to the plate separation problem for a power-law fluid is due to Scott.[11,12] Others, notably Leider and Bird,[13] Na[14] and more recently Grimm[15] have rederived Scott's equation. These authors have all considered the case where the fluid being squeezed fills the region between the plates, and is continuously ejected from the plate region during compression. The area of contact is thus always constant. In this work, a closely similar equation is derived but for the case of a sample of constant volume being compressed between two large plates. The derivation is given in Appendix A.

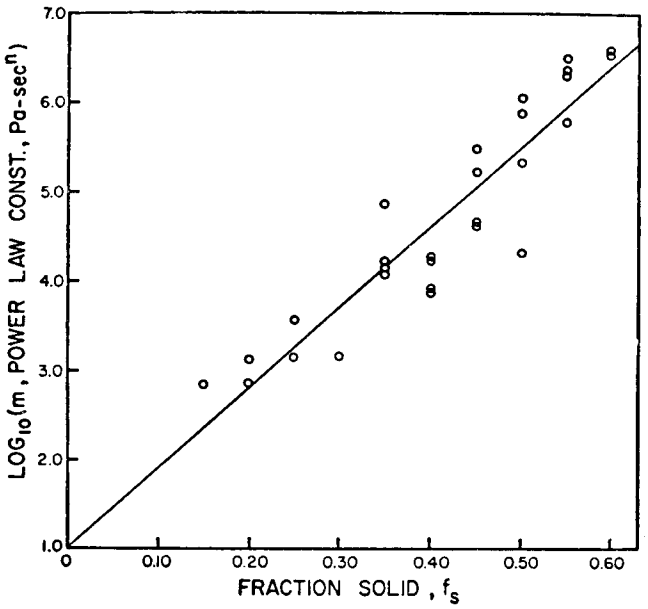

Fig. 15—Calculated values of power-law constant, *m*, *vs* fraction solid.

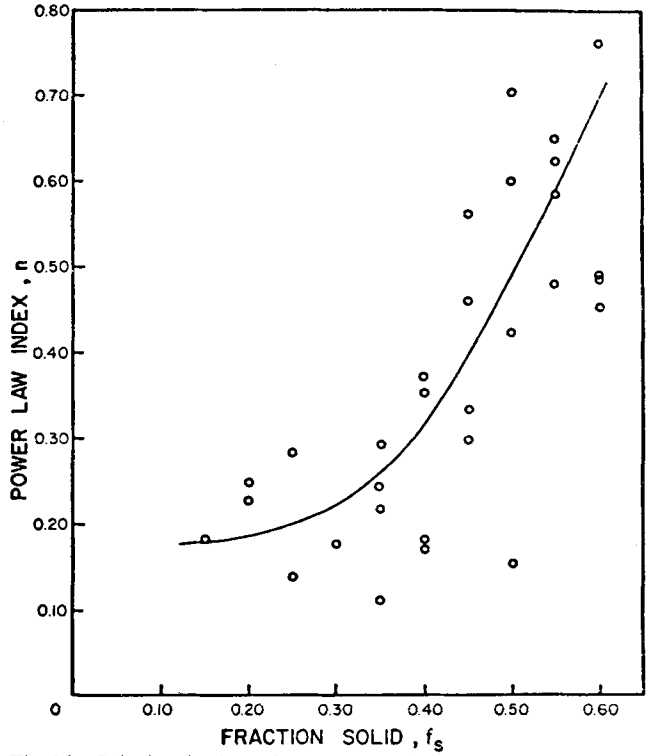

Fig. 16—Calculated values of power-law index, n, *vs* fraction solid.

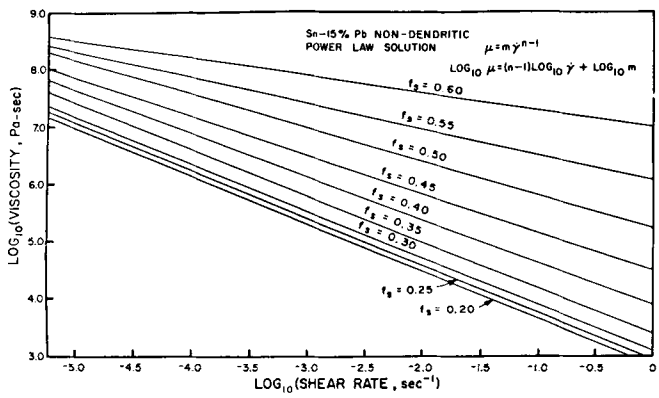

Fig. 17—Calculated viscosity *vs* shear rate according to the power-law equation using values of power-law parameters, m and n, based on experimental data in Figs. 15 and 16.

The final result is:

$$\frac{h_0}{h} = \left\{1 + \left(\frac{3n+5}{2n}\right) h_0^{(n+1)/n}\, kt\right\}^{2n/(3n+5)} \qquad [14]$$

where

$$k = \left\{\left(\frac{2n}{2n+1}\right)^n \frac{4F}{\pi d_0^{n+3} m}(n+3)\right\}^{1/n} \qquad [15]$$

Equation [14] is valid only in the limit $h \ll R$ which generally corresponds to long times of deformation.

Using these equations, it is possible to calculate the power-law parameters m and n for all the nondendritic experiments performed. Briefly, this involves replotting the experimental data using the following equation, valid for long times.

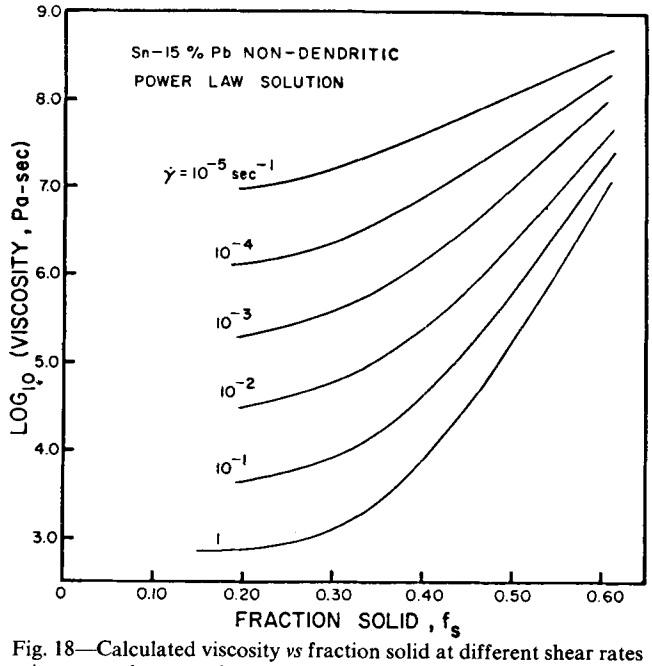

Fig. 18—Calculated viscosity *vs* fraction solid at different shear rates using power-law equation for partially remelted Sn-15 pct Pb nondendritic alloys.

$$\log(1-e) = -\frac{2n}{3n+5}\log t + \left\{-\left(\frac{2n}{3n+5}\right)\log\left(\frac{3n+5}{2n}\, h_0^{(n+1)/n}\, k\right)\right\} \qquad [16]$$

so that m and n may be obtained from the slope and intercept of a plot of $\log(1-e)$ *vs* $\log t$ at long times. The details of this analysis may be found in Appendix B. The calculated values of m are plotted in Fig. 15 as a function of fraction solid. The experimental points fall essentially on a straight line on a semilog plot and a least square fit yields:

$$m = 10.5 \exp(20.6 f_s) \quad 0.15 < f_s < 0.60 \qquad [17]$$

Figure 16 is a plot of the calculated values of n *vs* fraction solid. There is more scatter here than in the case of the parameter m, but for $f_s > 0.30$ the data may be adequately described by a straight line, yielding the following relationship between n and fraction solid, f_s,

$$n = -0.39 + 1.78 f_s \quad 0.30 < f_s < 0.60 \qquad [18]$$

Combining Eqs. [13], [17] and [18] yields the following relationship between viscosity, shear rate and fraction solid for the semisolid, nondendritic, Sn-15 pct Pb alloy,

$$\log\mu = 1.02 + 8.94 f_s + 1.78 f_s \log\dot{\gamma} - 1.39\log\dot{\gamma} \qquad [19]$$

or

$$\mu = a \exp(b f_s)\, \dot{\gamma}^{(cf_s+d)} \qquad [20]$$

where $a = 10.5$, $b = 20.6$, $c = 1.78$ and $d = -1.39$.

Equation [19] is plotted in Fig. 17. Note the close

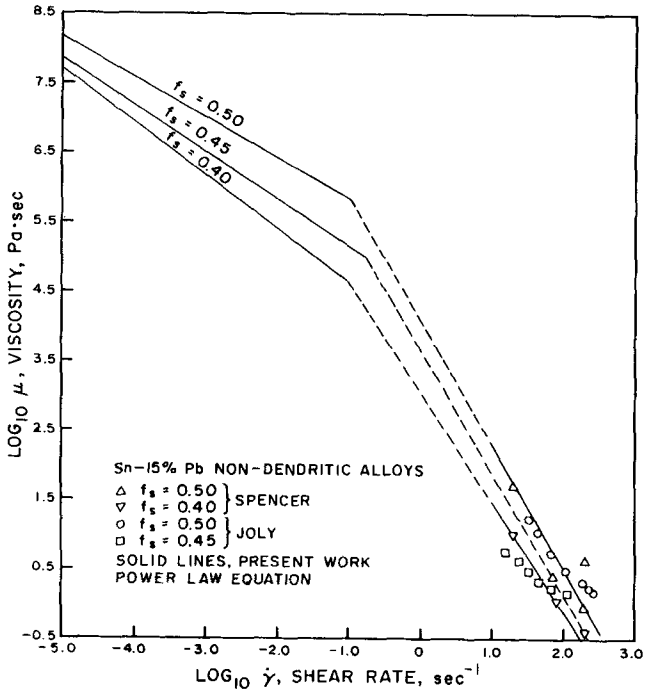

Fig. 19—Plot of viscosity *vs* shear rate for Sn-15 pct Pb nondendritic alloys. High shear rate data obtained from Rheocast slurries. Low shear rate data are for the remelted or Thixocast slurries.

quantitative agreement of the results obtained using this power law analysis with those obtained using the simpler Newtonian expressions (Fig. 13). Figure 18 plots the same data as μ *vs* f_s for different constant shear rates, that is, in a form comparable to the earlier data of Joly and Mehrabian in Fig. 1. Finally, Fig. 19 shows data from this work plotted on the same graph with earlier data of Joly and Mehrabian[9] and Spencer *et al*,[18] obtained at much higher shear rates. Note that if the data obtained in this work were extrapolated to the much higher shear rates of the earlier studies, the predicted viscosities would be much higher than those observed in the studies on Rheocast slurries. Stated differently, the "power law model" used herein, with constant coefficients m and n, is valid only over a limited range of shear rates ($10^{-5} < \dot{\gamma} < 10^{-1}$) and not over the entire seven orders of magnitude range in this figure.

DISCUSSION

In all suspensions reported in the literature, the power-law constant, m, increases with increasing vol pct solids.[21-29] This work shows similar results for the Sn-15 pct Pb Thixocast slurry.

In the case of the power-law index, n, rather different results are obtained. In particular, this appears to be the only reported instance of a pseudoplastic (or thixotropic) material where the index n increases with increasing fraction solid.

In many pseudoplastic suspensions (examples are $CaCo_3$ filled polypropylene, polystyrene/polypropylene blends and clay-water-oil slurries),[21-24] nearly parallel curves are obtained on a log-log plot of viscosity *vs* shear rate for different wt pct or vol pct of the second phase. Thus, in most pseudoplastic suspensions the power law index, n, is relatively independent of fraction solid. In most dilatant suspensions, however, (for example corn starch in glycerin)[25] the power-law index, n, is found to increase with vol pct solids. In other dilatant suspensions (such as TiO_2 in water, or sucrose solutions) n is relatively constant, especially at low shear rates; at high shear rates, the slope of the viscosity-shear rate plots change considerably and n is greatly influenced by vol pct solids.[26] Finally, in some pseudoplastic latexes (for example, polystyrene latex) the power-law index, n, increases with vol pct solids but in others such as Neoprene latex,[28,29] the power-law index, n, is a function of vol pct solids as well as the shear rate or shear stress.

It is also interesting that the semisolid "Thixocast" alloys exhibit pseudoplastic behavior at shear rates as low as 10^{-5} s^{-1}. Most polymers and other pseudoplastic materials become Newtonian at these low shear rates.

Finally, from an engineering standpoint it has been shown that extremely low forging pressures are needed to deform semisolid Thixocast alloys to very large strains. The forging pressures used in conventional forging of fully solid alloys are of the order of tens of thousands of pounds per square inch. For the Thixocast alloys studied here, the forging pressure is only of the order of tens of pounds per square inch, that is, lower by approximately three orders of magnitude. While the strain rates used in this investigation were about 1 to 2 orders of magnitude lower than the strain rates used in forging fully solid alloys, the fact that these Thixocast alloys are "pseudoplastic" or "thixotropic" would only improve the gains in forging pressures that may be obtained by using an initially Rheocast charge to forge industrial components at high strain rates.

CONCLUSIONS

1) Over the range of shear rates obtained in this investigation (10^{-5} to 10^{-1} s^{-1}), the semisolid Thixocast alloys are pseudoplastic and the viscosity decreases with increasing shear rates. The pseudoplastic behavior of these alloys may be described by the power-law model, $\mu = m\dot{\gamma}^{n-1}$.

2) The power-law parameters, m and n, may be obtained directly from an analysis of the long-time behavior of the measured strain-time curves.

3) Both the power-law parameters, m and n, increase with increasing fraction solid. The power-law constant, m, increases exponentially with fraction solid, f_s, being given by

$$m = a \exp(bf_s)$$

while the power-law index, n, increases following a linear relationship of the form,

$$n = cf_s + d$$

for fraction solids greater than about 0.30.

4) The forging pressures for the Thixocast alloys are about three orders of magnitude lower than the forging pressures used in forging fully solid alloys and about two orders of magnitude lower than forging pressures with semisolid dendritic alloys. The Thixocast alloys

deformed easily without cracking to very large strains while the dendritic alloys needed much higher loads, cracked easily and deformed with great difficulty.

APPENDIX A

Analysis of Strain-Time Relation for Power-Law Fluid Compressed Between Two Large Parallel Plates

For a power-law fluid,[13]

$$\tau_{rz} = -m \left| \frac{\partial v_r}{\partial z} \right|^{n-1} \frac{\partial v_r}{\partial z} \qquad [21]$$

where v_r is the radial velocity and m and n are constants.

Assuming $h \ll R$ (which normally corresponds to the limit of long times), the normal velocity of flow, v_z, can be neglected in comparison with the radial velocity, v_r. Also, from circular symmetry, v_θ is zero. With these assumptions, the basic equations for the flow field become,

$$\text{Continuity} \quad \frac{1}{r}\frac{\partial}{\partial r}(rv_r) + \frac{\partial v_z}{\partial z} = 0 \qquad [22]$$

$$\text{Momentum} \quad \frac{\partial P}{\partial r} = -m \frac{\partial}{\partial z}\left(-\frac{\partial v_r}{\partial z}\right)^n \qquad [23]$$

$$\frac{\partial P}{\partial z} = 0 \qquad [24]$$

With the boundary conditions

$$z = 0: \quad \partial v_r / \partial z(r,o) = 0 \qquad [25]$$

$$z = \frac{h}{2}: \quad v_z\left(r, \frac{h}{2}\right) = \frac{dh}{dt}$$

$$v_r\left(r, \frac{h}{2}\right) = 0 \qquad [26]$$

$$r = 0: \quad v_r(o,z) = 0 \qquad [27]$$

$$r = R: \quad p(R) = p_0 \qquad [28]$$

Equation [24] means that p is independent of z. Hence, integrating [23] twice with respect to z,

$$v_r = (-1)^{1/n}\left(\frac{n}{n+1}\right)\left(\frac{1}{m}\frac{dp}{dr}\right)^{1/n} \times \left[\left(\frac{h}{2}\right)^{(n+1)/n} - z^{(n+1)/n}\right] \qquad [29]$$

Next, integrating the continuity equation over z,

$$\frac{dh}{dt} = -\frac{2}{r}\frac{\partial}{\partial r}\left(r \int_0^{h/2} v_r dz\right) \qquad [30]$$

Integrating [30] over r

$$\frac{r}{2}\frac{dh}{dt} = -2 \int_0^{h/2} v_r dz \qquad [31]$$

Substituting [29] in [31] and integrating the pressure gradient so obtained gives,

$$p - p_0 = \left(\frac{m}{n+1}\right)(-1)^{n+1} \times \left\{\left(\frac{2n+1}{4n}\right)\left(\frac{h}{2}\right)^{-[(2n+1)/n]}\frac{dh}{dt}\right\}^n (r^{n+1} - R^{n+1}) \qquad [32]$$

Here R is radius of the specimen at time, t.

Integrating over the surface of the plates gives,

$$F = (-1)^n\left(\frac{m}{n+3}\right)\pi R^{n+3} \times \left\{\left(\frac{2n+1}{4n}\right)\left(\frac{h}{2}\right)^{-[(2n+1)/n]}\frac{dh}{dt}\right\}^n \qquad [33]$$

Since the fluid does not completely fill the space between the plates, R varies with time, t. However, since the volume is constant,

$$R^2 h = R_0^2 h_0$$

Substituting this in [33] and letting $d_0 = 2R_0$ gives,

$$-\frac{dh}{dt} = \left\{\left(\frac{2n}{2n+1}\right)^n \frac{4F}{\pi d_0^{n+3} m}(n+3)\right\}^{1/n} h_0^{-[(n+3)/2n]} h^{[5(n+1)/2n]} \qquad [34]$$

Let

$$k = \left\{\left(\frac{2n}{2n+1}\right)^n \frac{4F}{\pi d_0^{n+3} m}(n+3)\right\}^{1/n} \qquad [35]$$

Thus,

$$-\frac{dh}{dt} = k h_0^{-[(n+3)/2n]} h^{[5(n+1)/2n]} \qquad [36]$$

Integrating from $h = h_0$ at $t = 0$

$$\left(\frac{1}{h}\right)^{(3n+5)/2n} - \left(\frac{1}{h_0}\right)^{(3n+5)/2n} = \left(\frac{3n+5}{2n}\right) k h_0^{-[(n+3)/2n]} t \qquad [37]$$

For $n = 1$, $m = \mu$ this reduces to Eq. [6] in the text.

The shear rate, $\dot{\gamma}$, at any point (r,z) within the fluid is given by

$$\dot{\gamma} = -\frac{\partial v_r}{\partial z} = -\frac{2(dh/dt)}{h^2}\left(\frac{2n+1}{2n}\right)\left(\frac{z}{h/2}\right)^{1/n} r \qquad [38]$$

For $n = 1$, this reduces to the Newtonian shear rate quoted in the text, Eq. [8].

Rewriting [37],

$$\frac{h_0}{h} = \left\{1 + \left(\frac{3n+5}{2n}\right) h_0^{(n+1)/n} kt\right\}^{2n/(3n+5)} \qquad [39]$$

Equation [39] is the modified form of Scott's equation for the case where the fluid does not completely fill the space between the plates. The original Scott equation, applicable where the fluid completely fills the space is,

$$\frac{h_0}{h} = \left\{1 + \left(\frac{n+1}{n}\right) h_0^{(n+1)/n}\, kt\right\}^{n/(n+1)} \quad [40]$$

The engineering strain, e, is given by

$$e = \left(1 - \frac{h}{h_0}\right)$$

$$= 1 - \left\{1 + \left(\frac{3n+5}{2n}\right) h_0^{(n+1)/n}\, kt\right\}^{-[2n/(3n+5)]} \quad [41]$$

Equation [41] is the theoretical strain-time curve for a power-law fluid.

Let $t = t_{1/2}$ when $h = h_0/2$. Then from [39],

$$\frac{Fh_0}{d_0^3} = k_0\left(\frac{d_0/h_0}{t_{1/2}}\right)^n \quad [42]$$

where

$$k_0 = \frac{\pi}{4} m \left(\frac{2n+1}{3n+5}\right)\left(\frac{2^{(3n+5)/2n} - 1}{n}\right)\left(\frac{1}{n+3}\right)^{1/n} \quad [43]$$

APPENDIX B

Determination of Power-Law Parameters m and n from Experimental Data

Equations [36], [41] and [42] suggest three independent methods of determining the power-law parameters n and m.

Method I

From [36]

$$\log_{10}\left(-\frac{dh}{dt}\right) = \frac{5(n+1)}{2n}\log_{10} h + \log_{10}\{kh_0^{-[(n+3)/2n]}\} \quad [44]$$

Hence, a plot of $\log_{10}(-dh/dt)$ *vs* $\log_{10} h$ should yield a straight line with a slope of $[5(n+1)]/2n$. The intercept at $\log_{10} h = 0$ gives the values of m. This method has been discussed by Oka[20] and Van Wazer *et al*[31] but no experimental results were presented. Gandhi and Burns[32] used a modified form of this equation to determine the power-law parameters for glass-filled DMC in a constant strain-rate experiment.

Method II

Rewriting Eq. [42]

$$\log_{10}\left(\frac{Fh_0}{d_0^3}\right) = \log_{10} k_0 + n\log_{10}\left(\frac{d_0/h_0}{t_{1/2}}\right) \quad [45]$$

so that a plot of $\log(Fh_0/d_0^3)$ *vs* $\log[(d_0/h_0)/t_{1/2}]$ should yield a straight line with a slope n for a power-law fluid. Leider and Bird[33] used this method to determine m and n for a hydroxyethylcellulose solution. According to these authors only a single point on the strain curve $(h_0/2, t_{1/2})$ is necessary to determine m and n and a complete analysis of the strain curve is unnecessary, as in Method I.

Method III

From Eq. [41]

$$\ln(1-e) = -\left(\frac{2n}{3n+5}\right) \times \ln\left\{1 + \left(\frac{3n+5}{2n}\right) h_0^{(n+1)/n}\, kt\right\} \quad [46]$$

For $1 \ll ([3n+5]/2n)\, h_0^{(n+1)/n}\, kt$, *i.e.* at long times,

$$\ln(1-e) = -\left(\frac{2n}{3n+5}\right)\ln t - \left(\frac{2n}{3n+5}\right)\ln\left(\frac{3n+5}{2n} h_0^{(n+1)/n}\, k\right) \quad [47]$$

which is of the form,

$$\ln(1-e) = a \ln t + b \quad [48]$$

Hence a plot of $\ln(1-e)$ *vs* $\ln t$ should yield a straight line at long times; n being obtained from the slope of this line and m from the intercept at $\ln(1-e) = 0$. This approach allows the power-law parameters to be obtained directly from the measured strain-time curves and does not seem to have been used previously. The m and n values plotted in Figs. 15 and 16 were calculated using this long time approximation, Eq. [48].

ACKNOWLEDGMENT

This work was supported by the National Science Foundation, Grant. No. DMR 78-10905.

REFERENCES

1. M. C. Flemings and R. Mehrabian: *Trans. Am. Foundrymen's Soc.*, 1973, vol. 81, p. 81. (Also *Trans. Int. Foundry Congr., Moscow.*)
2. M. C. Flemings, R. G. Riek, and K. P. Young: *AFS Int. Cast Met. J.*, 1976, vol. 1, no. 3, p. 11.
3. Rheocasting, Metals and Ceramics Information Center, Report, January 1978.
4. S. D. E. Ramati, G. J. Abbaschian, D. G. Backman, and R. Mehrabian: *Met. Trans. B*, 1978, vol. 9B, p. 279.
5. K. P. Young, R. G. Riek, J. F. Boylan, R. L. Bye, B. E. Bond, and M. C. Flemings: *Trans. Am. Foundrymen's Soc.*, 1976, vol. 84, p. 169 (also, *Die Cast. Eng.*, March–April, 1976, p. 46). Presented at 80th AFS Congress, Chicago, IL, 1976.
6. K. P. Young, R. G. Riek and M. C. Flemings: *Trans. SDCE*, 1977, vol. 9, paper GT-77-092.

7. M. C. Flemings, J. F. Boylan and R. L. Bye: Final Technical Report, ARPA Contract No. DAAG-46-77-C-0033, prepared for Army Materials and Mechanics Research Center, Watertown, MA 02172.
8. D. B. Spencer, R. Mehrabian, and M. C. Flemings: *Met. Trans.*, 1972, vol. 3, p. 1925.
9. P. A. Joly and R. Mehrabian: *J. Mater. Sci.*, 1976, vol. 11, p. 1393.
10. G. H. Dienes and H. F. Klemm: *J. Appl. Phys.*, 1946, vol. 17, p. 458.
11. J. R. Scott: *Trans. IRI*, 1931, vol. 7, p. 169.
12. J. R. Scott: *Trans. IRI*, 1932, vol. 8, p. 481.
13. P. J. Leider and R. B. Bird: *Ind. Eng. Chem. Fund.*, 1974, vol. 13, p. 336.
14. T. Y. Na: *J. Basic Eng.*, 1966, vol. 88, p. 687.
15. R. J. Grimm: *AIChEJ*, 1978, vol. 24, p. 427.
16. W. M. Gearhart and W. D. Kennedy: *Ind. Eng. Chem.*, April 1949, p. 695.
17. M. C. Flemings, *et al*: Interim Technical Report, ARPA Contract No. DAAG-46-C-0010, 1973, prepared for Army Materials and Mechanics Research Center, Watertown, MA 02172.
18. M. C. Flemings, *et al*: Interim Technical Report, ARPA Contract No. DAAG-46-C-0010, 1974, prepared for Army Materials and Mechanics Research Center, Watertown, MA 02172.
19. J. F. Stefan: *Versuche Uber Die Scheinbare Adhasion Sitzber M th. Naturw. kl. Bagar Akad. Wiss Munchen*, 1974, vol. 69, part 2.
20. S. Oka: *Rheology*, F. R. Eirich, ed., vol. 3, pp. 18–82, Academic Press, New York, 1960.
21. C. D. Han: *Rheology in Polymer Processing*, pp. 165–191, Academic Press, London, 1976.
22. C. D. Han: *J. Appl. Polymer Sci.*, 1974, vol. 18, p. 481.
23. J. C. Reed, M.S. Thesis, University of Delaware, Newark, DE, 1954.
24. C. D. Han and Y. W. Kim: *J. Appl. Polymer Sci.*, 1975, vol. 19, p. 2831.
25. R. G. Green and R. G. Griskey: *Trans. Soc. Rheol.*, 1968, vol. 12, pp. 13 and 27.
26. A. B. Metzner and M. Whitlock: *Trans. Soc. Rheol.*, 1958, vol. 2, p. 239.
27. S. H. Maron and A. L. Pascal: *J. Colloid Sci.*, 1955, vol. 10, p. 434.
28. I. M. Krieger and S. H. Maron: *J. Colloid Sci.*, 1951, vol. 6, p. 582.
29. S. H. Maron and R. J. Belner: *J. Colloid Sci.*, 1955, vol. 10, p. 523.
30. V. Laxmanan: Sc.D. Thesis, Department of Materials Science and Engineering, Massachusetts Institute of Technology, Cambridge, MA, January 1979.
31. J. R. Van Wazer, J. W. Lyons, K. Y. Kim and R. E. Colwell: *Viscosity and Flow Measurements*, pp. 292–95, Interscience, New York, 1963.
32. K. S. Gandhi and R. Burns: *Trans. Soc. Rheol.*, 1976, vol. 20, p. 489.
33. P. J. Leider and R. B. Bird: *Ind. Eng. Chem. Fund.*, 1974, vol. 13, p. 348.